

Transition from s_{\pm} -wave to $d_{x^2-y^2}$ -wave superconductivity driven by interlayer interaction in the bilayer two-orbital model of $\text{La}_3\text{Ni}_2\text{O}_7$

Wenhan Xi,¹ Shun-Li Yu,^{1,2,*} and Jian-Xin Li^{1,2,†}

¹National Laboratory of Solid State Microstructures and Department of Physics, Nanjing University, Nanjing 210093, China

²Collaborative Innovation Center of Advanced Microstructures, Nanjing University, Nanjing 210093, China

(Dated: March 20, 2025)

We utilize the fluctuation-exchange approximation on a bilayer two-orbital model, incorporating $d_{x^2-y^2}$ and d_{z^2} orbitals, to explore potential pairing symmetries in the bilayer nickelate $\text{La}_3\text{Ni}_2\text{O}_7$. Our study particularly examines the impact of interlayer Coulomb interactions. In the absence of these interactions, the superconducting gap exhibits s_{\pm} -wave symmetry, with predominant intra-orbital pairing in the d_{z^2} orbital. As interlayer interactions increase, s_{\pm} -wave superconductivity is suppressed, while the superconductivity with a $d_{x^2-y^2}$ -wave gap is enhanced, resulting in a transition at a critical interaction strength. This $d_{x^2-y^2}$ -wave superconductivity is distinct not only from the s_{\pm} -wave superconductivity but also from the intraorbital d -wave pairing in cuprate superconductors, as it is dominated by the interlayer pairing between the $d_{x^2-y^2}$ and d_{z^2} orbitals. Additionally, charge fluctuations play a crucial role in driving the transition from s_{\pm} wave to $d_{x^2-y^2}$ wave superconductivity. Our findings indicate that interlayer Coulomb interactions are crucial for understanding the pairing mechanism in $\text{La}_3\text{Ni}_2\text{O}_7$.

I. INTRODUCTION

Since the discovery of high-temperature superconductivity in cuprates, the mechanisms underlying this phenomenon and the search for new superconducting materials have remained some of the most challenging and significant topics in condensed matter physics. Recently, the discovery of superconductivity with a transition temperature $T_c \approx 80$ K under high pressure in the nickelate $\text{La}_3\text{Ni}_2\text{O}_7$ [1–9] has marked the first instance of achieving high-temperature superconductivity within the liquid nitrogen temperature range in non-cuprate materials. This breakthrough has spurred intensive research activity into Ni-based superconductors.

At ambient pressure, $\text{La}_3\text{Ni}_2\text{O}_7$ is metallic and exhibits an orthorhombic structure. Upon increasing the pressure, it undergoes a structural transition from the Amm to the $Fmmm$ at approximately 14 GPa [1, 10], coinciding with the onset of superconductivity. Above T_c , the resistivity shows a linear temperature dependence [1–3], highlighting the importance of electronic correlations. Although there is no consensus on the precise magnetic properties of this material from experimental studies, techniques such as resonant inelastic X-ray scattering [11], muon-spin relaxation [12, 13], nuclear magnetic resonance [14, 15], and neutron scattering [16] all suggest the presence of magnetic ordering or significant magnetic fluctuations. Additionally, a charge density wave may also exist and influence the physical properties of $\text{La}_3\text{Ni}_2\text{O}_7$ [17, 18]. These findings imply that magnetic and charge fluctuations could be crucial in understanding the pairing mechanism in this material.

Since it is not feasible to probe the band structure at

high pressure using angle-resolved photoemission spectroscopy, all current theoretical studies on the superconducting mechanism in $\text{La}_3\text{Ni}_2\text{O}_7$ rely on results from density functional theory (DFT) calculations [1, 19–25]. DFT results under high pressure reveal that the low energy bands near the Fermi level are predominantly composed of Ni-3 $d_{x^2-y^2}$ and Ni-3 d_{z^2} orbitals. This has consequently led to the widespread adoption of the bilayer two-orbital model in theoretical studies [22–25]. However, some researches have proposed that the band structure of $\text{La}_3\text{Ni}_2\text{O}_7$ is analogous to that of the bilayer cuprates, leading to the use of a bilayer single-orbital model as well [26]. Additionally, certain studies also suggest that in the strong coupling limit, the two-orbital model can be approximated as a single-orbital model [27].

A variety of methods have been used to explore the nature of superconducting pairing symmetry, including the functional renormalization group (fRG), tensor network calculations, random phase approximation (RPA), and dynamical mean-field theory (DMFT) [24–47]. Theoretical results vary significantly based on the models and methods applied. In studies using a two-orbital model with $d_{x^2-y^2}$ and d_{z^2} orbitals, fRG [28], RPA [31, 47] and DMFT [37, 40] studies suggested an s_{\pm} -wave symmetry driven by inter-pocket spin fluctuations. One study also revealed that minor adjustments to the crystal field splitting (~ 0.2 eV) can switch the dominant symmetry between s_{\pm} to d_{xy} [47], highlighting the sensitivity of pairing symmetry to low-energy electronic structures. Conversely, bilayer single-orbital models predominantly predict d -wave pairing mediated by antiferromagnetic spin fluctuations [26]. A slave-boson mean-field analysis of the bilayer single-orbital t - J - J_{\perp} models revealed that strong interlayer magnetic exchange J_{\perp} tunes the single-layer d -wave superconducting state to the s -wave one with dominant interlayer pairings [27], a result also supported by tensor network calculations [36].

Although there is currently no consensus on the pair-

* slyu@nju.edu.cn

† jxli@nju.edu.cn

ing symmetry of $\text{La}_3\text{Ni}_2\text{O}_7$ in theoretical researches, with both s -wave and d -wave pairing symmetries being proposed, almost all studies indicate that the interlayer coupling of the $\text{Ni-}3d_{z^2}$ orbital plays a crucial role in determining the pairing symmetry. Given the strong interlayer coupling of the $\text{Ni-}3d_{z^2}$ orbital, it naturally leads us to ponder whether the interlayer Coulomb interactions of the $3d_{z^2}$ orbital could also play a significant role in determining the pairing symmetry. While some studies have discussed the impact of interlayer superexchange on superconductivity [27, 29, 36], most previous research has focused primarily on intralayer Coulomb interactions, often neglecting the interlayer aspects. Therefore, analyzing the influence of interlayer Coulomb interactions on pairing symmetry may be crucial for revealing the superconducting pairing mechanism of $\text{La}_3\text{Ni}_2\text{O}_7$.

In this paper, we employ a bilayer two-orbital model consisting of $d_{x^2-y^2}$ and d_{z^2} orbitals, using the fluctuation-exchange (FLEX) approximation to study the potential superconducting pairing symmetries of $\text{La}_3\text{Ni}_2\text{O}_7$. We pay particular attention to the effects of the interlayer Coulomb interaction V_z between the d_{z^2} orbitals. For $V_z = 0$, we find that the superconducting gap exhibits s_{\pm} -wave symmetry, with dominant intraorbital pairing of the d_{z^2} orbital and similar amplitudes for both intralayer and interlayer pairings. As V_z increases, the s_{\pm} -wave superconductivity is gradually suppressed, while the $d_{x^2-y^2}$ -wave superconductivity is enhanced, leading to a transition to the $d_{x^2-y^2}$ -wave superconductivity at a critical V_z . During this process, charge fluctuations associated with V_z play a critical role. Moreover, unlike the s_{\pm} -wave superconductivity, the $d_{x^2-y^2}$ -wave superconductivity is dominated by the interlayer pairing between the $d_{x^2-y^2}$ and d_{z^2} orbitals. Furthermore, due to the mirror symmetry of the bilayer structure, pairing symmetries can also be described using the bonding-antibonding basis. In this framework, the s_{\pm} -wave superconductivity is dominated by intraorbital pairing of the antibonding d_{z^2} orbital, while the $d_{x^2-y^2}$ -wave superconductivity is dominated by interorbital pairing between the bonding $d_{x^2-y^2}$ and d_{z^2} orbitals.

The paper is organized as follows: In section II, we introduce the model and the FLEX method, highlighting some unique properties of the model. Section III details the evolution of superconducting pairing symmetries and thoroughly discusses the underlying mechanisms. Section IV presents a summary.

II. MODEL AND METHOD

Based on DFT calculations predicting dominant $\text{Ni-}3d_{x^2-y^2}$ and $\text{Ni-}3d_{z^2}$ characteristics near the Fermi level [22–25, 34], we employ the following effective bilayer

two-orbital tight-binding (TB) model [22]:

$$H_0 = \sum_{\substack{i\delta, ll' \\ aa', \sigma}} t_{ll', aa'}^\delta c_{ila\sigma}^\dagger c_{i+\delta, l'a'\sigma} - \sum_{ila\sigma} (\varepsilon_a + \mu) n_{ila\sigma}, \quad (1)$$

where $c_{ila\sigma}$ is the electron annihilation operator associated with site i , layer $l = \{A, B\}$, orbital $a = \{x, z\}$ and spin σ . $n_{ila\sigma} = c_{ila\sigma}^\dagger c_{ila\sigma}$ is the particle number operator. The layers are labeled A and B , while the $d_{x^2-y^2}$ and d_{z^2} orbitals are denoted by x and z . The parameter $\delta = \{1, 2\}$ represents the nearest-neighbor (NN) and next-nearest-neighbor (NNN) hoppings, and μ is the chemical potential. We adopt the TB parameters from Luo et al. in Ref. 22. The onsite energies are $(\varepsilon_x, \varepsilon_z) = (-0.776, -0.409)$ eV. The intralayer hoppings are $(t_{ll', xx}^1, t_{ll', xx}^2, t_{ll', zz}^1, t_{ll', zz}^2, t_{ll', xz}^1) = (-0.483, 0.069, -0.11, -0.017, 0.239)$ eV, and the interlayer hoppings are $(t_{ll', xz}^1, t_{ll', xx}^1, t_{ll', zz}^1) = (-0.034, 0.005, -0.635)$ eV for $l \neq l'$. The significant interlayer hopping of the d_{z^2} orbital and the strong intralayer hybridization between different orbitals indicate that neither the two orbitals nor the two layers can be simply decoupled. These are key features of the TB model.

We can transform the Hamiltonian (1) into momentum space as follows:

$$H_0 = \sum_{\mathbf{k}\sigma} \Psi_{\mathbf{k}\sigma}^\dagger M(\mathbf{k}) \Psi_{\mathbf{k}\sigma}, \quad (2)$$

where $\Psi_{\mathbf{k}\sigma} = (c_{kAx\sigma}, c_{kAz\sigma}, c_{kBx\sigma}, c_{kBz\sigma})^T$, and $M(\mathbf{k})$ is a 4×4 Hermitian matrix. Here, $c_{kla\sigma}$ is the Fourier transformation from $c_{ila\sigma}$, and the elements of $M(\mathbf{k})$ are derived from the Fourier transformation of the Hamiltonian (1).

The band structure and Fermi surface (FS) of the model (1) with chemical potential $\mu = 0$ are shown in Fig. 1(a) and (b), respectively. This choice of chemical potential corresponds to the nominal $3d^{7.5}$ electronic configuration in $\text{La}_3\text{Ni}_2\text{O}_7$ [1], where the three t_{2g} orbitals are fully filled and the two e_g orbitals have an average occupancy of 1.5 electrons. In this bilayer two-orbital model, this is equivalent to an average filling of 3 electrons per site. There are three sets of FS: an electron pocket α near the Γ point, and a hole pocket β and a hole pocket γ around the M point. The small γ pocket is predominantly composed of d_{z^2} orbital, whereas the α and β pockets arise from the hybridization of $d_{x^2-y^2}$ and d_{z^2} orbitals. Additionally, the FS depicted in Fig. 1(b) features two distinct sets of nesting wave vectors, denoted by \mathbf{Q}_1 and \mathbf{Q}_2 , which are expected to lead to strong spin and charge fluctuations.

Due to the mirror symmetry of the bilayer structure, the matrix $M(\mathbf{k})$ in Eq. (2) can be expressed as a block diagonal matrix in the bonding-antibonding (BA) basis:

$$H_0 = \sum_{\mathbf{k}\sigma} \tilde{\Psi}_{\mathbf{k}\sigma}^\dagger \tilde{M}(\mathbf{k}) \tilde{\Psi}_{\mathbf{k}\sigma}. \quad (3)$$

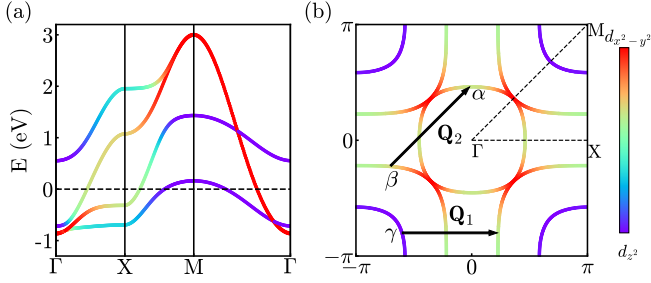


FIG. 1. Band structure (a) and Fermi surface (b) of the bilayer two-orbital model. Colors indicate orbital weights. The three Fermi pockets in (b) are labeled α , β , and γ . Black arrows \mathbf{Q}_1 and \mathbf{Q}_2 in (b) denote the nesting wave vectors.

Here, $\tilde{\Psi}_{\mathbf{k}\sigma} = (c_{k,+x\sigma}, c_{k,+z\sigma}, c_{k,-x\sigma}, c_{k,-z\sigma})^T$, where $c_{k,\pm,a\sigma} = (c_{kAa\sigma} \pm c_{kB a\sigma})/\sqrt{2}$ represents the bonding and antibonding states. The matrix $\tilde{M}(\mathbf{k})$ is given by

$$\tilde{M}(\mathbf{k}) = U^\dagger M(\mathbf{k})U, \quad (4)$$

where

$$U = \frac{1}{\sqrt{2}} \begin{pmatrix} 1 & 0 & 1 & 0 \\ 0 & 1 & 0 & 1 \\ 1 & 0 & -1 & 0 \\ 0 & 1 & 0 & -1 \end{pmatrix} \quad (5)$$

is the transformation matrix from the orbital-layer representation to the BA representation. Since there is no mixing between the bonding and antibonding states, the α and γ pockets are derived entirely from the bonding states, while the β pocket is derived entirely from the antibonding states. As illustrated in Fig. 1, the bonding state of the d_{z^2} orbital is predominantly on the γ pocket, whereas the antibonding state of the d_{z^2} orbital is mainly on the β pocket. The bonding state of the $d_{x^2-y^2}$ orbital is confined to the α pocket, while its antibonding state is located on the β pocket. These distributions of the bonding and antibonding orbitals impose significant constraints on the superconducting pairing symmetry, as we will discuss below.

The strong interlayer hopping of the d_{z^2} orbital suggests that interlayer superconducting pairing in this orbital is also likely to be significant, potentially making interlayer interactions crucial for determining the pairing symmetry. However, previous theoretical studies often overlooked these interlayer interactions [2, 24–28, 31–40, 42–45]. By considering both intralayer and interlayer interactions, we derive the following interaction form:

$$H_{int} = H_{intra} + H_{inter}, \quad (6)$$

where

$$\begin{aligned} H_{intra} = & \frac{U}{2} \sum_{il,a,\sigma \neq \sigma'} n_{ila\sigma} n_{ila\sigma'} + \frac{U'}{2} \sum_{il,\sigma\sigma',a \neq a'} n_{ila\sigma} n_{ila'\sigma'} \\ & + \frac{J}{2} \sum_{il,a \neq a',\sigma\sigma'} c_{ila\sigma}^\dagger c_{ila'\sigma'}^\dagger c_{ila\sigma} c_{ila'\sigma} \\ & + \frac{J'}{2} \sum_{il,a \neq a',\sigma \neq \sigma'} c_{ila\sigma}^\dagger c_{ila\sigma'}^\dagger c_{ila'\sigma'} c_{ila'\sigma} \end{aligned} \quad (7)$$

and

$$H_{inter} = \frac{V_z}{2} \sum_{i,l \neq l',\sigma\sigma'} n_{ilz\sigma} n_{il'z\sigma'}. \quad (8)$$

Here, U (U') is the intraorbital (interorbital) Coulomb interaction, J is the Hund's coupling, and J' is the interorbital pairing hopping, all within a layer. V_z denotes the interlayer Coulomb interaction of the d_{z^2} orbital. In our calculations, the relations $U = U' + 2J$ and $J = J'$ are used.

Given recent experiments suggesting the possible presence of spin and charge density waves in $\text{La}_3\text{Ni}_2\text{O}_7$ at ambient pressure [11–14, 16, 17], spin and charge fluctuations are likely to play a crucial role in superconducting pairing under high pressure. To explore this, we employ the FLEX approximation [48–51], a self-consistent conserving method that is particularly effective for studying superconductivity mediated by various collective fluctuations. For the bilayer two-orbital model, the Green's function and self-energy are expressed as 4×4 matrices, satisfying:

$$G^{-1}(k) = G_0^{-1}(k) - \Sigma(k) \quad (9)$$

and

$$\Sigma_{mn}(k) = \frac{T}{N} \sum_{q,uv} V_{nu,mv}(q) G_{uv}(k-q), \quad (10)$$

where each subscript combines layer (l) and orbital (a) indices, e.g., $m = (l_m, a_m)$. Here, T represents the temperature, $k = (\mathbf{k}, i\omega_n)$ with Matsubara frequency $\omega_n = (2n+1)\pi T$, and N is the total number of lattice sites. The bare Green's function is given by $G_0(k) = [i\omega_n - M(\mathbf{k})]^{-1}$. The interaction vertex V is represented as a 16×16 matrix:

$$\begin{aligned} V(q) = & \frac{3}{2} U^s [\chi^s(q) - \chi^0(q)] U^s + \frac{1}{2} U^c [\chi^c(q) - \chi^0(q)] U^c \\ & + \frac{1}{2} [U^s \chi^0(q) U^s + U^c \chi^0(q) U^c] \end{aligned} \quad (11)$$

with spin susceptibility $\chi^s(q) = [1 - \chi^0(q) U^s]^{-1} \chi^0(q)$ and charge susceptibility $\chi^c(q) = [1 + \chi^0(q) U^c]^{-1} \chi^0(q)$. The irreducible susceptibility is given by

$$\chi_{mn,uv}^0(q) = -\frac{T}{N} \sum_k G_{um}(k+q) G_{nv}(k). \quad (12)$$

The matrices U^s and U^c are defined as follows: for $a_m = a_n = a_u = a_v$ and $l_m = l_n = l_u = l_v$, $U_{mn,uv}^s = U$, $U_{mn,uv}^c = U$; for $a_m = a_u \neq a_n = a_v$ and $l_m = l_n = l_u = l_v$, $U_{mn,uv}^s = U'$, $U_{mn,uv}^c = 2J - U'$; for $a_m = a_n \neq a_u = a_v$ and $l_m = l_n = l_u = l_v$, $U_{mn,uv}^s = J$, $U_{mn,uv}^c = 2U' - J$; for $a_m = a_v \neq a_n = a_u$ and $l_m = l_n = l_u = l_v$, $U_{mn,uv}^s = J'$, $U_{mn,uv}^c = J'$; for $a_m = a_u = a_n = a_v = d_{z^2}$ and $l_m = l_n \neq l_u = l_v$, $U_{mn,uv}^s = V_z$, $U_{mn,uv}^c = -V_z$; for $a_m = a_u = a_n = a_v = d_{z^2}$ and $l_m = l_n \neq l_u = l_v$, $U_{mn,uv}^s = 0$, $U_{mn,uv}^c = 2V_z$; for other cases, $U_{mn,uv}^s = 0$, $U_{mn,uv}^c = 0$. These equations are solved self-consistently with $N = 64 \times 64$ \mathbf{k} -point meshes and 1024 ω_n .

Assuming that the pairing interaction responsible for superconductivity arises from the exchange of spin and charge fluctuations, we can derive the effective pairing interaction using the FLEX approximation [48–50]. The singlet pairing interaction is given by

$$\begin{aligned} \Gamma(q) &= \Gamma^s(q) + \Gamma^c(q) + \Gamma^0(q) \\ &= \frac{3}{2} U^s \chi^s(q) U^s - \frac{1}{2} U^c \chi^c(q) U^c + \frac{1}{2} (U^s + U^c). \end{aligned} \quad (13)$$

In this expression, Γ^s , Γ^c and Γ^0 represent the contributions from spin fluctuations, charge fluctuations, and the zero-order term, respectively. The superconducting pairing functions can be obtained by solving the Eliashberg equation:

$$\lambda \phi_{ij}(k) = -\frac{T}{N} \sum_{p, mn, uv} \Gamma_{mijn}(k-p) G_{mu}(p) G_{nv}(-p) \phi_{uv}(p). \quad (14)$$

The eigenvector $\phi(k)$ with the largest eigenvalue λ indicates the most favorable superconducting pairing symmetry.

The symmetries of the $d_{x^2-y^2}$ and d_{z^2} orbitals impose a specific constraint on the pairing functions. Under reflection across the line $y = x$ (or $y = -x$), the matrix $M(\mathbf{k})$ in Hamiltonian (2) satisfies the relation:

$$M(\hat{R}\mathbf{k}) = U_R^\dagger M(\mathbf{k}) U_R, \quad (15)$$

where \hat{R} represents the reflection across the line $y = x$ and $U_R = \text{diag}(1, -1, 1, -1)$. The bands, obtained by diagonalizing $M(\mathbf{k})$ with a unitary transformation $U_b(\mathbf{k})$, remain invariant under the reflection \hat{R} . Thus, the matrix $U_b(\mathbf{k})$ satisfies $U_b(\hat{R}\mathbf{k}) = U_R U_b(\mathbf{k})$. The gap function $\Delta(\mathbf{k})$ in the band representation, obtained from $\phi(\mathbf{k})$ in the orbital-layer representation using the matrix $U_b(\mathbf{k})$ via $\Delta(\mathbf{k}) = U_b^\dagger(\mathbf{k}) \phi(\mathbf{k}) U_b(\mathbf{k})$, must satisfy $\Delta(\hat{R}\mathbf{k}) = \pm \Delta(\mathbf{k})$. Consequently, the pairing function $\phi(k)$ satisfies:

$$\phi(\hat{R}\mathbf{k}) = \pm U_R \phi(\mathbf{k}) U_R. \quad (16)$$

This imposes a strong constraint on the pairing function: if the intraorbital pairings do not change sign under the transformation \hat{R} , then the interorbital pairings must change sign, and vice versa. This constraint applies to both the orbital-layer and BA representations.

III. RESULTS AND DISCUSSION

In this section, we explore how pairing symmetry evolves with changes in interaction parameters. For convenience, in the orbital-layer representation, the orbital and layer indices (Ax, Az, Bx, Bz) are denoted as (1, 2, 3, 4). In the BA representation, the indices ($x+, z+, x-, z-$) are denoted as (x, z, \bar{x}, \bar{z}).

A. The case for $V_z = 0$

Let's begin with the situation where there are no inter-layer interactions, i.e., $V_z = 0$, and set $U = 1.0$ eV. We have verified that the results for $U = 0.5$ eV and $U = 1.5$ eV are qualitatively consistent with those for $U = 1.0$ eV. The chemical potential is set to $\mu = 0$, corresponding to the case of $\text{La}_3\text{Ni}_2\text{O}_7$, with an average electron density per site of $n = 3$ in the bilayer two-orbital model (1). In Fig. 2(a)-(c), we present the three main components of the pairing function $\phi(\mathbf{k})$. It is evident that the dominant pairings are the intralayer pairing ϕ_{22} and the interlayer pairing ϕ_{24} of the d_{z^2} orbitals, both having nearly the same magnitude. These pairings maintain their signs throughout the entire Brillouin zone (BZ), exhibiting s -wave characteristics, but with opposite signs. In contrast, as shown in Fig. 2(c), the interorbital pairing between the $d_{x^2-y^2}$ and d_{z^2} orbitals is dominated by the intralayer component ϕ_{12} and exhibits $d_{x^2-y^2}$ -wave characteristics. These features of the pairing function satisfy the constraint condition (16) well. The pairing function can be explicitly expressed as:

$$\phi_{ij}(\mathbf{k}) = \begin{cases} \Delta_\alpha & ij = 22 \text{ or } 44 \\ \Delta_\beta & ij = 24 \\ \Delta_\gamma (\cos k_x - \cos k_y) & ij = 12 \text{ or } 34 \\ 0 & \text{otherwise} \end{cases} \quad (17)$$

with $\Delta_\alpha : \Delta_\beta : \Delta_\gamma = 1 : -1.11 : 0.17$ and $\phi_{ij}(\mathbf{k}) = \phi_{ji}(\mathbf{k})$. Upon projecting the gap function onto the FS, as illustrated in Fig. 2(d), it is observed that the gap functions on the α and γ pockets are essentially opposite in sign compared to that on the β pocket, indicating characteristics of s_\pm -wave symmetry, consistent with the other recent theoretical studies, including fRG, RPA and DMFT approaches using similar bilayer two-orbital models [28–41]. These characteristics also suggest that the superconducting pairing is predominantly in the d_{z^2} orbital and exhibits strong interlayer pairing. This is a significant departure from results obtained from bilayer single-orbital models [27, 36], where superconducting pairing mainly occurs in the $d_{x^2-y^2}$ orbitals.

To gain a more comprehensive understanding of the origin of the s_\pm -wave superconducting gap shown in Fig. 2(d), we utilize the BA representation. The mirror symmetry ensures that there is no mixing between the bonding and antibonding states. Specifically, the α and γ pockets are composed of bonding states, while the β

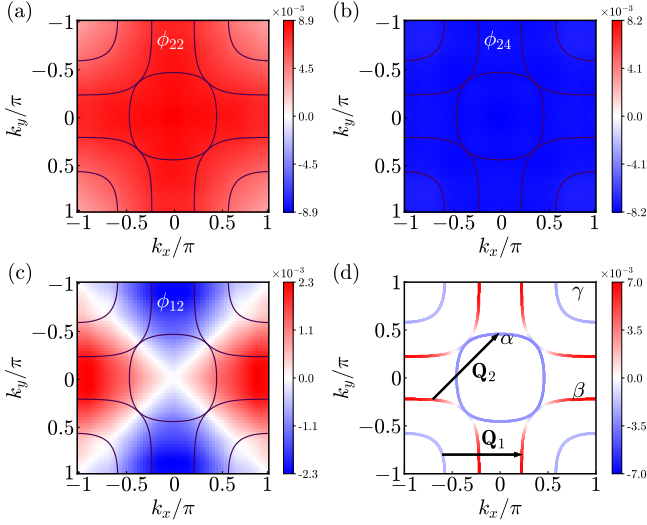


FIG. 2. Pairing functions for $U = 1.0$ eV and $V_z = 0$ in the orbital-layer representation. (a) Intralayer pairing ϕ_{22} for the d_{z^2} orbital. (b) Interlayer pairing ϕ_{24} for the d_{z^2} orbital. (c) Intralayer pairing ϕ_{12} between the $d_{x^2-y^2}$ and d_{z^2} orbitals. (d) Gap Function projected onto the Fermi surface, with black arrows \mathbf{Q}_1 and \mathbf{Q}_2 indicating sign changes.

pocket arises from antibonding states. For Cooper pairs with zero center-of-mass momentum, there is no pairing between bonding and antibonding states. This separation is highly advantageous for analyzing the structure of the gap function.

As illustrated in Fig. 3(a)-(e), within the BA representation, the pairing functions adhere to constraint (16), just as in the orbital-layer representation [Fig. 2(a)-(c)]. The pairing function $\tilde{\phi}_{\bar{z}\bar{z}}$ [Fig. 3(a)], associated with the antibonding state of the d_{z^2} orbital, exhibits the largest pairing magnitude, significantly exceeding other pairing components. Since the antibonding state of the d_{z^2} orbital contributes solely to the β pocket, this results in the superconducting gap on the β pocket having the maximal value [Fig. 2(d)]. We also observed that the superconducting gap on the β pocket is not uniform and contains nodes, whereas the pairing function $\tilde{\phi}_{\bar{z}\bar{z}}$ is almost uniform throughout the BZ. This discrepancy arises due to the contribution of the antibonding state of the $d_{x^2-y^2}$ orbital. As shown in Fig. 3(b), the pairing function $\tilde{\phi}_{\bar{x}\bar{x}}$, associated with the antibonding state of the $d_{x^2-y^2}$ orbital, exhibits an opposite sign to $\tilde{\phi}_{\bar{z}\bar{z}}$. Although $\tilde{\phi}_{\bar{x}\bar{x}}$ is much smaller than $\tilde{\phi}_{\bar{z}\bar{z}}$, the weight of the $d_{x^2-y^2}$ orbital is significantly greater than that of the d_{z^2} orbital in the Γ - M direction [Fig. 1(b)], leading to a change in sign of the superconducting gap on the β pocket and consequently the presence of a node.

Another important feature of the gap function, as shown in Fig. 2(d), is the sign change between the bonding pockets (α and γ) and the antibonding pocket (β), indicated by the vectors \mathbf{Q}_1 and \mathbf{Q}_2 . Since there is no pairing between bonding and antibonding states, ana-

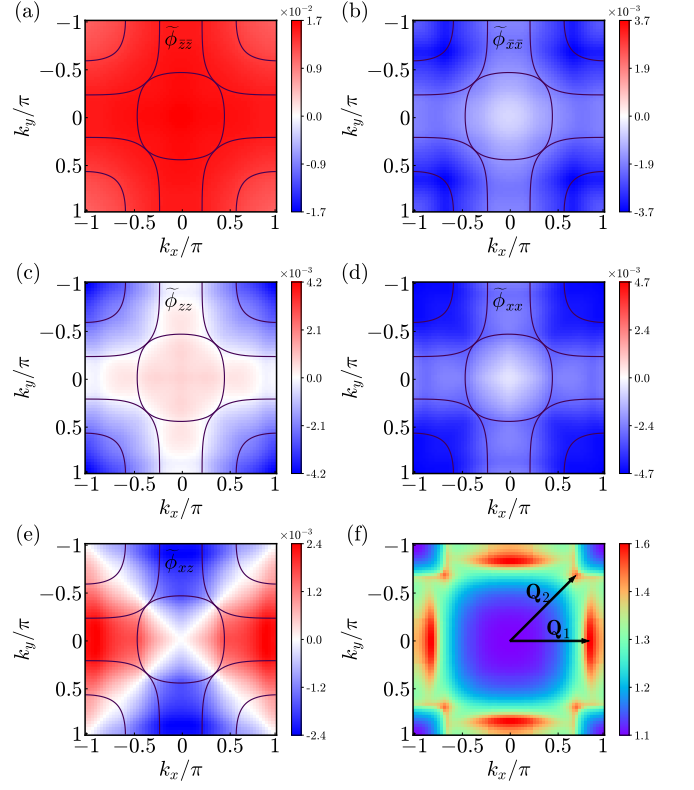


FIG. 3. Pairing functions and pairing interaction in the bonding-antibonding representation for $U = 1.0$ eV and $V_z = 0$. (a)-(e) Pairing functions. (f) Pairing interaction $\tilde{\Gamma}_{z\bar{z}\bar{z}\bar{z}}(\mathbf{k})$, with black arrows \mathbf{Q}_1 and \mathbf{Q}_2 indicating peaks.

lyzing the sign changes of the gap function under the BA representation becomes much simpler. The pairing equation in the BA representation can be derived from equation (14) using the transformation (5). For the bonding and antibonding states of the d_{z^2} orbital, the pairing functions satisfy the following relation:

$$\lambda_{\tilde{\phi}_{\bar{z}\bar{z}}}(\mathbf{k}) \sim -\frac{T}{N} \sum_{\mathbf{q}} \tilde{\Gamma}_{z\bar{z}\bar{z}\bar{z}}(\mathbf{q}) \tilde{G}_{z\bar{z}}(\mathbf{k}-\mathbf{q}) \tilde{G}_{z\bar{z}}(\mathbf{q}-\mathbf{k}) \times \tilde{\phi}_{z\bar{z}}(\mathbf{k}-\mathbf{q}). \quad (18)$$

As shown in Fig. 3(f), the pairing interaction $\tilde{\Gamma}_{z\bar{z}\bar{z}\bar{z}}$ peaks at the wave vector \mathbf{Q}_1 , originating from enhanced spin and charge fluctuations due to FS nesting between the β and γ pockets [see Fig. 1(b)]. This means that the pairing scatterings are dominated by transitions from $(\mathbf{k}, -\mathbf{k})$ to $(\mathbf{k} + \mathbf{Q}_1, -\mathbf{k} - \mathbf{Q}_1)$. To achieve a maximal λ , the pairing function must satisfy the condition $\tilde{\phi}_{\bar{z}\bar{z}}(\mathbf{k}) \tilde{\phi}_{z\bar{z}}(\mathbf{k} - \mathbf{Q}_1) < 0$ [see Eq. (18)]. This results in the bonding and antibonding states of the d_{z^2} orbital, connected by \mathbf{Q}_1 [Fig. 2(d)], having opposite signs [Figs. 3(a) and (c)]. Consequently, the gap functions on the β and γ pockets also exhibit opposite signs. In the BA representation, $\tilde{\Gamma}_{z\bar{z}\bar{z}\bar{z}}$ is the dominant component of the effective pairing interaction $\tilde{\Gamma}(\mathbf{q})$. Its secondary peaks, indicated

by the wave vector \mathbf{Q}_2 originating from FS nesting between the α and β pockets [see Fig. 1(b)], also determine that the gap functions on the α and β pockets have opposite signs. The α pocket is mainly associated with the bonding state of the $d_{x^2-y^2}$ orbital [Fig. 1(b)]. The pairing functions $\tilde{\phi}_{\bar{z}\bar{z}}$ and $\tilde{\phi}_{xx}$ follow this relation:

$$\lambda \tilde{\phi}_{\bar{z}\bar{z}}(\mathbf{k}) \sim -\frac{T}{N} \sum_{\mathbf{q}} \tilde{\Gamma}_{z\bar{z}z\bar{z}}(\mathbf{q}) \tilde{G}_{zx}(\mathbf{k}-\mathbf{q}) \tilde{G}_{zx}(\mathbf{q}-\mathbf{k}) \times \tilde{\phi}_{xx}(\mathbf{k}-\mathbf{q}). \quad (19)$$

Thus, $\tilde{\phi}_{\bar{z}\bar{z}}$ and $\tilde{\phi}_{xx}$ must satisfy $\tilde{\phi}_{\bar{z}\bar{z}}(\mathbf{k})\tilde{\phi}_{xx}(\mathbf{k}-\mathbf{Q}_2) < 0$, which results in the bonding state of the $d_{x^2-y^2}$ orbital and the antibonding state of the d_{z^2} orbital, linked by \mathbf{Q}_2 [Fig. 2(d)], having opposite signs [Figs. 3(a) and (d)]. Consequently, the gap functions on the α and β pockets also display opposite signs.

We also find that in the BA representation, the spin fluctuations $\tilde{\chi}_{z\bar{z}z\bar{z}}^s$ and $\tilde{\chi}_{x\bar{x}x\bar{x}}^s$ dominate the effective pairing interaction $\tilde{\Gamma}_{z\bar{z}z\bar{z}}$ among various collective fluctuations. According to Eqs. (13) and (5), their contributions to $\tilde{\Gamma}_{z\bar{z}z\bar{z}}$ can be expressed as:

$$\tilde{\Gamma}_{z\bar{z}z\bar{z}} \sim U^2 \tilde{\chi}_{z\bar{z}z\bar{z}}^s + J^2 \tilde{\chi}_{x\bar{x}x\bar{x}}^s. \quad (20)$$

As illustrated in Figs. 8(a) and (b) in Appendix A, $\tilde{\chi}_{z\bar{z}z\bar{z}}^s$ and $\tilde{\chi}_{x\bar{x}x\bar{x}}^s$ are responsible for the two peaks of $\tilde{\Gamma}_{z\bar{z}z\bar{z}}$ at \mathbf{Q}_1 and \mathbf{Q}_2 , respectively.

B. The case for $V_z = 0.5$ eV

Next, we explore how the interlayer interaction V_z affects the superconducting pairing symmetry, with a particular focus on the results for $U = 1.0$ eV and $V_z = 0.5$ eV. Figures 4(a)-(c) illustrate the three main components of $\phi(\mathbf{k})$, which differ from the primary components observed when $V_z = 0$ [see Figs. 2(a)-(c)]. The interlayer pairing ϕ_{14} between the $d_{x^2-y^2}$ and d_{z^2} orbitals, along with the intralayer pairing ϕ_{11} of the $d_{x^2-y^2}$, become the primary pairing components. As shown in Fig. 4(d), the gap function projected onto the FS exhibits a $d_{x^2-y^2}$ -wave symmetry, contrasting with the s_{\pm} -wave symmetry observed when $V_z = 0$. This pairing functions can be approximately expressed as:

$$\phi_{ij}(k) = \begin{cases} \Delta_{\alpha} & ij = 14 \text{ or } 23, \\ \Delta_{\beta 1}(\cos k_x - \cos k_y) & \\ + \Delta_{\beta 2}(\cos 2k_x - \cos 2k_y) & ij = 11 \text{ or } 33, \\ 0 & \text{otherwise,} \end{cases} \quad (21)$$

where $\Delta_{\alpha} : \Delta_{\beta 1} : \Delta_{\beta 2} = 1 : -0.48 : -0.15$ and $\phi_{ij}(k) = \phi_{ji}(k)$. Although the symmetries of the pairing functions in this case are entirely different from those for $V_z = 0$, they still satisfy constraint condition (16). In addition, this d -wave superconductivity is dominated by interlayer pairing between the $d_{x^2-y^2}$ and d_{z^2} orbitals, which significantly differs from the d -wave superconductivity dominated by intralayer pairing within the

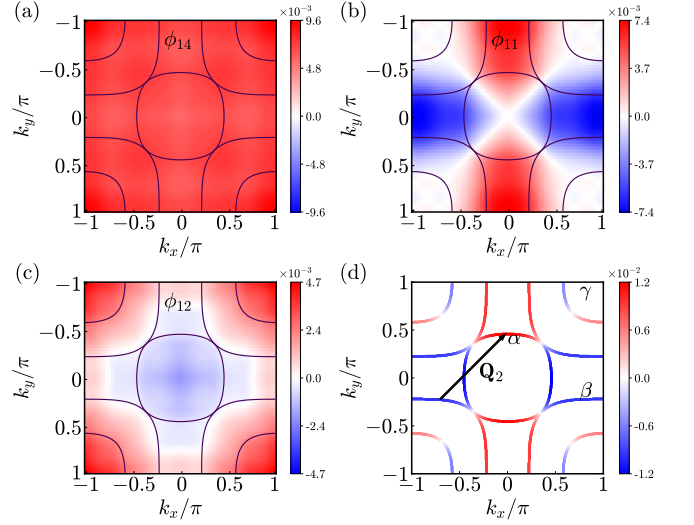


FIG. 4. Pairing functions for $U = 1.0$ eV and $V_z = 0.5$ eV in the orbital-layer representation. (a) Interlayer pairing ϕ_{14} between the $d_{x^2-y^2}$ and d_{z^2} orbitals. (b) Intralayer pairing ϕ_{11} for the $d_{x^2-y^2}$ orbital. (c) Intralayer pairing ϕ_{12} between the $d_{x^2-y^2}$ and d_{z^2} orbitals. (d) Gap Function projected onto the Fermi surface, with black arrow \mathbf{Q}_2 indicating sign change.

$d_{x^2-y^2}$ orbital in cuprate superconductors. The interorbital and interlayer characteristics of this d -wave superconductivity also differ markedly from the d -wave superconductivity based on the $d_{x^2-y^2}$ single-orbital model for $\text{La}_3\text{Ni}_2\text{O}_7$ [26, 27], which exhibits a single-layer d -wave pairing.

Using the same approach applied to the s_{\pm} -wave superconducting state at $V_z = 0$, we employ the BA representation to investigate the origin of $d_{x^2-y^2}$ -wave state at $V_z = 0.5$ eV. In Figs. 5(a)-(d), we display the main components of the pairing function $\tilde{\phi}(\mathbf{k})$. We find that, for both the bonding and antibonding states, the dominant pairing is interorbital, which contrasts sharply with the $V_z = 0$ situation, where the intraorbital pairings are predominant [Figs. 3(a)-(d)]. Notably, the intraorbital pairing of the d_{z^2} orbital is no longer favorable due to the interlayer repulsive interaction V_z . Furthermore, we find that the pairing functions $\tilde{\phi}_{xz}$ and $\tilde{\phi}_{\bar{x}\bar{z}}$ for bonding and antibonding states, respectively, have opposite signs. This can be explained by the following relation:

$$\lambda \tilde{\phi}_{\bar{x}\bar{z}}(\mathbf{k}) \sim -\frac{T}{N} \sum_{\mathbf{q}} \tilde{\Gamma}_{x\bar{x}z\bar{z}}(\mathbf{q}) \tilde{G}_{zx}(\mathbf{k}-\mathbf{q}) \tilde{G}_{zx}(\mathbf{q}-\mathbf{k}) \times \tilde{\phi}_{xz}(\mathbf{k}-\mathbf{q}). \quad (22)$$

As illustrated in the Fig. 5(e), the interorbital pairing interaction $\tilde{\Gamma}_{x\bar{x}z\bar{z}}$ peaks at the wave vector \mathbf{Q}_2 . This results in $\tilde{\phi}_{xz}$ and $\tilde{\phi}_{\bar{x}\bar{z}}$ satisfying $\tilde{\phi}_{xz}(\mathbf{k})\tilde{\phi}_{\bar{x}\bar{z}}(\mathbf{k}-\mathbf{Q}_2) < 0$, leading to the opposite signs of $\tilde{\phi}_{xz}$ and $\tilde{\phi}_{\bar{x}\bar{z}}$. Similarly, the intraorbital pairing functions $\tilde{\phi}_{xx}$ and $\tilde{\phi}_{\bar{x}\bar{x}}$ satisfy the

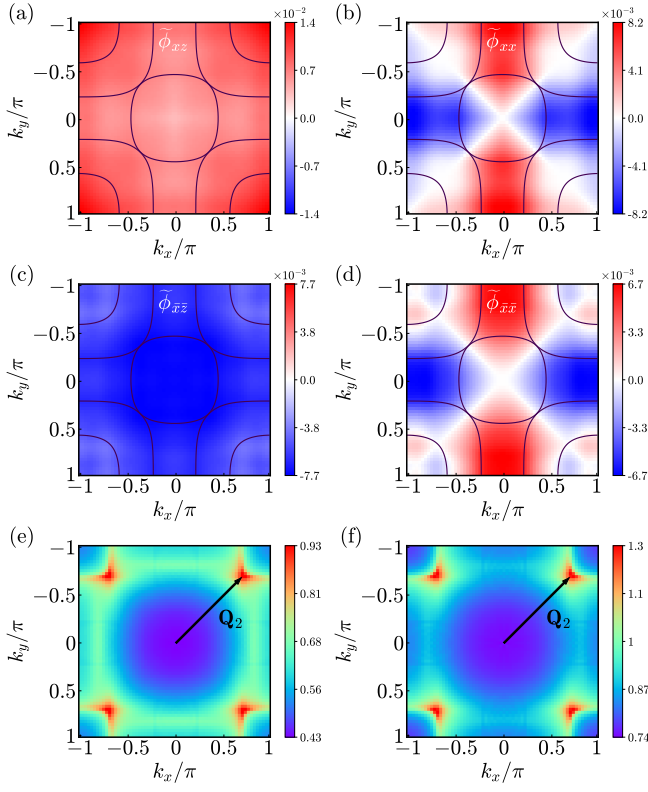


FIG. 5. Pairing function and pairing interaction in the bonding-antibonding representation for $U = 1.0$ eV and $V_z = 0.5$ eV. (a)-(d) Pairing functions. (e) Pairing interaction $\tilde{\Gamma}_{x\bar{x}\bar{z}\bar{z}}(\mathbf{k})$. (f) Pairing interaction $\tilde{\Gamma}_{x\bar{x}\bar{x}\bar{x}}(\mathbf{k})$. The black arrows \mathbf{Q}_2 in (e) and (f) indicating peaks.

following relation:

$$\lambda \tilde{\phi}_{\bar{x}\bar{x}}(\mathbf{k}) \sim -\frac{T}{N} \sum_{\mathbf{q}} \tilde{\Gamma}_{x\bar{x}\bar{x}\bar{x}}(\mathbf{q}) \tilde{G}_{xx}(\mathbf{k}-\mathbf{q}) \tilde{G}_{xx}(\mathbf{q}-\mathbf{k}) \times \tilde{\phi}_{xx}(\mathbf{k}-\mathbf{q}). \quad (23)$$

As depicted in the Fig. 5(f), $\tilde{\Gamma}_{x\bar{x}\bar{x}\bar{x}}$ has a similar structure to $\tilde{\Gamma}_{x\bar{x}\bar{z}\bar{z}}$, resulting in opposite signs for the bonding-state pairing $\tilde{\phi}_{xx}$ and the antibonding-state pairing $\tilde{\phi}_{\bar{x}\bar{x}}$, linked by \mathbf{Q}_2 [Figs. 5(b) and (d)]. These sign changes between the bonding-state and antibonding-state pairings collectively result in the gap function exhibiting d -wave symmetry, as shown in Fig. 4(d).

Similar to the case when $V = 0$, for $V_z = 0.5$ eV, the effective pairing interactions are also primarily driven by spin fluctuations. The two key effective pairing interactions $\tilde{\Gamma}_{x\bar{x}\bar{z}\bar{z}}$ and $\tilde{\Gamma}_{x\bar{x}\bar{x}\bar{x}}$ discussed above are primarily governed by the spin fluctuations $\tilde{\chi}_{\bar{x}\bar{x}\bar{z}\bar{z}}^s$ and $\tilde{\chi}_{x\bar{x}\bar{x}\bar{x}}^s$ [see Figs. 8(c) and (d) in Appendix A], respectively. According to Eqs. (13) and (5), the relationships between them are:

$$\tilde{\Gamma}_{x\bar{x}\bar{z}\bar{z}} \sim U(U + V_z) \tilde{\chi}_{\bar{x}\bar{x}\bar{z}\bar{z}}^s \quad (24)$$

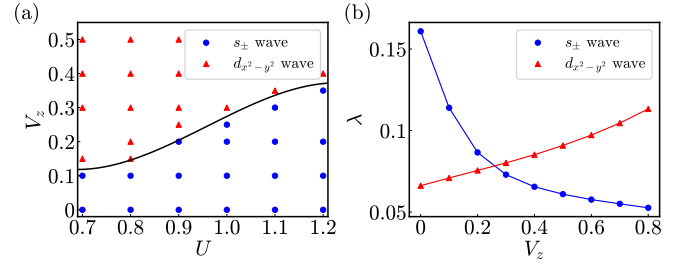


FIG. 6. (a) U - V_z phase diagram of pairing symmetry. The solid line represents the critical value for the superconducting transition. (b) Dependence of λ on V_z for s_{\pm} -wave and $d_{x^2-y^2}$ -wave pairings at $U = 1.0$ eV.

and

$$\tilde{\Gamma}_{x\bar{x}\bar{x}\bar{x}} \sim U^2 \tilde{\chi}_{x\bar{x}\bar{x}\bar{x}}^s. \quad (25)$$

C. Evolution of pairing symmetry with interactions

We then examine how the pairing symmetry evolves with variations in the on-site Hubbard interaction U and the interlayer Coulomb interaction V_z . The phase diagram for pairing symmetry in the (U, V_z) parameter space, obtained using the FLEX method, is shown in Fig. 6(a). For small values of V_z , the pairing symmetry is s_{\pm} -wave. However, as V_z increases, the $d_{x^2-y^2}$ -wave superconducting state becomes more favorable. The critical value of V_z for the transition from the s_{\pm} -wave state to the $d_{x^2-y^2}$ -wave state increases with U .

As illustrated in Fig. 6(b), the eigenvalue λ in Eq. (14) for the s_{\pm} -wave state decreases with increasing V_z , whereas the eigenvalue for the $d_{x^2-y^2}$ -wave state increases. With the rise of V_z , the component $\tilde{\Gamma}_{zzzz}$ of pairing interaction $\tilde{\Gamma}(\mathbf{q})$ changes significantly more than the other components. As depicted in Figs. 7(a) and (b), the introduction of V_z leads to a substantial increase in $\tilde{\Gamma}_{zzzz}$, with its peak shifting to $\mathbf{Q}_3 = (\pi, \pi)$. Considering the following relation:

$$\lambda \tilde{\phi}_{zz}(\mathbf{k}) \sim -\frac{T}{N} \sum_{\mathbf{q}} \tilde{\Gamma}_{zzzz}(\mathbf{q}) \tilde{G}_{zz}(\mathbf{k}-\mathbf{q}) \tilde{G}_{zz}(\mathbf{q}-\mathbf{k}) \times \tilde{\phi}_{zz}(\mathbf{k}-\mathbf{q}), \quad (26)$$

it is clear that $\tilde{\Gamma}_{zzzz}$ tends to favor $\tilde{\phi}_{zz}(\mathbf{k}) \tilde{\phi}_{zz}(\mathbf{k}-\mathbf{Q}_3) < 0$, requiring $\tilde{\phi}_{zz}$ to have a d -wave form. In contrast, the constrain condition (16) restricts $\tilde{\phi}_{zz}$ to an s -wave form for the s_{\pm} -wave state. Consequently, the increase of V_z suppresses the s_{\pm} -wave state. This aligns with the observation in real space that the interlayer interaction V_z can suppress the primary d_{z^2} -orbital interlayer pairing in Eq. (17).

To understand why an increase in V_z benefits the $d_{x^2-y^2}$ -wave state, we analyze how the three pairing amplitudes in Eq. (21) evolve with V_z . As shown in Fig. 7(c),

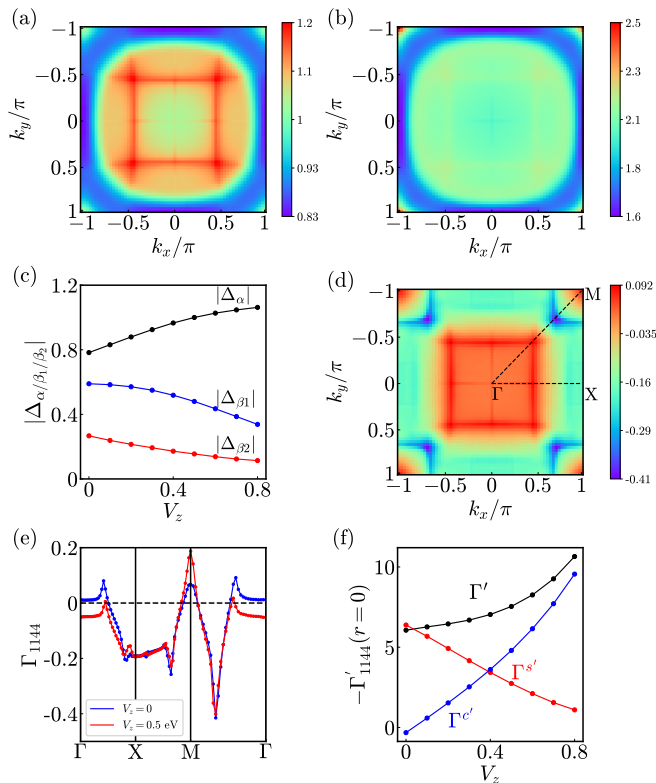


FIG. 7. (a) Pairing interaction $\tilde{\Gamma}_{zzzz}$ for $V_z = 0$. (b) $\tilde{\Gamma}_{zzzz}$ for $V_z = 0.5$ eV; (c) Evolution of the pairing amplitudes in Eq. (21) as a function of V_z . (d) Pairing interaction Γ_{1144} for $V_z = 0$. (e) Intensities of the pairing interaction Γ_{1144} along high-symmetry lines shown in (d) for both $V_z = 0$ and $V_z = 0.5$ eV. (f) Evolution of the pairing potential $\Gamma'_{1144}(\mathbf{r} = 0)$ and the contributions of the spin and charge fluctuations with varying V_z .

only the amplitude Δ_α increases, while the others decrease. This suggests that the pairing components ϕ_{14} and ϕ_{41} become increasingly dominant as V_z rises. Thus, to understand how V_z enhances the $d_{x^2-y^2}$ -wave state, we can examine its effect on ϕ_{14} and ϕ_{41} using the following relation in the orbital-layer representation:

$$\lambda\phi_{14}(\mathbf{k}) \sim -\frac{T}{N} \sum_{\mathbf{q}} \Gamma_{1144}(\mathbf{q}) G_{14}(\mathbf{k} - \mathbf{q}) G_{41}(\mathbf{q} - \mathbf{k}) \times \phi_{41}(\mathbf{k} - \mathbf{q}). \quad (27)$$

The interorbital pairing interaction Γ_{1144} between the $d_{x^2-y^2}$ and d_{z^2} orbitals on different layers for $V_z = 0$ is depicted in Fig. 7(d). A key feature of Γ_{1144} is its predominance of negative values. This generally requires ϕ_{14} to maintain its sign across the entire BZ, characteristic of the $d_{x^2-y^2}$ -wave state [see Fig. 4(a)]. As illustrated in Fig. 7(e), with increasing V_z , the negative region of Γ_{1144} , which favors $d_{x^2-y^2}$ -wave state, also expands. Thus, an increase in V_z promotes the emergence of $d_{x^2-y^2}$ -wave superconductivity. To clarify this further, we perform a Fourier transform on $\Gamma_{1144}(\mathbf{q})$ to obtain the effective

pairing potential $\Gamma'_{1144}(\mathbf{r})$ in real space. We find that $\Gamma'_{1144}(\mathbf{r} = 0)$ acts as an attractive interaction for two electrons on the same site, consistent with the s -wave form of ϕ_{14} . In Fig. 7(f), we demonstrate the evolution of $\Gamma'_{1144}(\mathbf{r} = 0)$ along with the contributions from spin and charge fluctuations ($\Gamma^{s'}(\mathbf{r} = 0)$ and $\Gamma^{c'}(\mathbf{r} = 0)$) as a function of V_z . The functions $\Gamma^{s'}(\mathbf{r})$ and $\Gamma^{c'}(\mathbf{r})$ are obtained via Fourier transformations of $\Gamma_{1144}^s(\mathbf{q})$ and $\Gamma_{1144}^c(\mathbf{q})$ as described in Eq. (13). It is observed that the charge-fluctuation contribution $\Gamma^{c'}(\mathbf{r} = 0)$ becomes dominant as V_z increases. Specially, according to Eq. (13), the effects of V_z on Γ_{1144}^c can be simplified as:

$$\Gamma_{1144}^c \sim -U_{1122}^c \chi_{2222}^c U_{2244}^c = -2V_z(2U' - J)\chi_{2222}^c. \quad (28)$$

We find that the charge fluctuation of d_{z^2} orbital (χ_{2222}^c) plays a crucial role in affecting the evolution of Γ_{1144}^c with V_z and consequently plays a crucial role in the realization of $d_{x^2-y^2}$ -wave superconductivity.

IV. SUMMARY

Motivated by the strong interlayer coupling in the bilayer nickelate $\text{La}_3\text{Ni}_2\text{O}_7$, we investigated the impact of interlayer Coulomb interactions on superconducting pairing symmetry. Using the fluctuation-exchange approximation on a bilayer two-orbital model with $d_{x^2-y^2}$ and d_{z^2} orbitals, we found that the interlayer Coulomb interaction V_z between the d_{z^2} orbitals can induce a change in the superconducting gap from s_{\pm} -wave symmetry to $d_{x^2-y^2}$ -wave symmetry. In the s_{\pm} -wave superconducting state with small V_z , the dominant pairing is intraorbital within the d_{z^2} orbital, exhibiting similar amplitudes for both intralayer and interlayer components. Conversely, in the $d_{x^2-y^2}$ -wave superconducting state with large V_z , the leading pairing involves interlayer interactions between the $d_{x^2-y^2}$ and d_{z^2} orbitals. In the s_{\pm} -wave superconducting state, intraorbital pairing components exhibit s -wave symmetry, while interorbital components exhibit d -wave symmetry. In contrast, in the $d_{x^2-y^2}$ -wave superconducting state, intraorbital components show d -wave symmetry, and interorbital components show s -wave symmetry. Additionally, the mirror symmetry of the bilayer structure allows us to describe pairing symmetries using a bonding-antibonding basis. In this context, the s_{\pm} -wave superconductivity primarily involves intraorbital pairing within the antibonding d_{z^2} orbital, whereas the $d_{x^2-y^2}$ -wave superconductivity is mainly characterized by interorbital pairing between the bonding $d_{x^2-y^2}$ and d_{z^2} orbitals.

ACKNOWLEDGMENTS

This work was supported by National Key Projects for Research and Development of China (No. 2024YFA1408104 and No. 2021YFA1400400) and

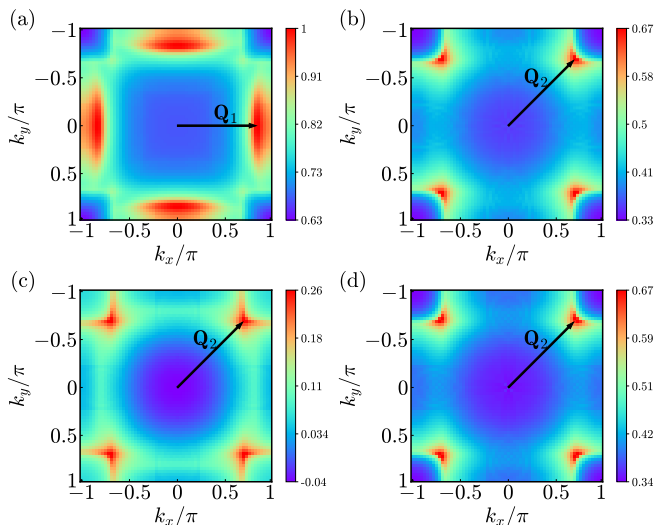


FIG. 8. Susceptibilities in the BA representation. (a) $\tilde{\chi}_{zzzz}^s$ for $V_z = 0$. (b) $\tilde{\chi}_{xx\bar{x}\bar{x}}^s$ for $V_z = 0$. (c) $\tilde{\chi}_{xx\bar{z}\bar{z}}^s$ for $V_z = 0.5$ eV. (d) $\tilde{\chi}_{x\bar{x}\bar{x}\bar{x}}^s$ for $V_z = 0.5$ eV.

the National Natural Science Foundation of China

(No. 12074175, No. 92165205, No. 12374137, and No. 12434005).

Appendix A: Spin susceptibilities

In the FLEX approximation, the effective pairing interactions stem from various collective fluctuations. In the model we explore in this paper, spin fluctuations play a dominant role. We present the spin susceptibilities $\tilde{\chi}_{zzzz}^s$ and $\tilde{\chi}_{xx\bar{x}\bar{x}}^s$ in Figs. 8(a) and (b), which primarily contribute to the effective interaction $\tilde{\Gamma}_{zzzz}$ at $V_z = 0$. Similarly, the spin susceptibilities $\tilde{\chi}_{xx\bar{z}\bar{z}}^s$ and $\tilde{\chi}_{x\bar{x}\bar{x}\bar{x}}^s$ shown in Figs. 8(c) and (d) are key contributors to the effective interactions $\tilde{\Gamma}_{xx\bar{z}\bar{z}}$ and $\tilde{\Gamma}_{x\bar{x}\bar{x}\bar{x}}$ at $V_z = 0.5$ eV. Here, $\tilde{\chi}^s$ represents the spin susceptibility in the BA representation, which can be derived from χ^s in the orbital-layer representation using the transformation matrix U in Eq. (5). The peaks in these susceptibilities, indicated by Q_1 and Q_2 , originate from the nesting properties between the bonding and antibonding pockets of FS, as shown in Fig. 1(b).

-
- [1] H. Sun, M. Huo, X. Hu, J. Li, Z. Liu, Y. Han, L. Tang, Z. Mao, P. Yang, B. Wang, J. Cheng, D.-X. Yao, G.-M. Zhang, and M. Wang, Signatures of superconductivity near 80 K in a nickelate under high pressure, *Nature* **621**, 493 (2023).
- [2] Y. Zhang, L.-F. Lin, A. Moreo, T. A. Maier, and E. Dagotto, High-temperature superconductivity with zero resistance and strange-metal behaviour in $\text{La}_3\text{Ni}_2\text{O}_{7-\delta}$, *Nat. Commun.* **15**, 2470 (2024).
- [3] Y. Zhang, D. Su, Y. Huang, Z. Shan, H. Sun, M. Huo, K. Ye, J. Zhang, Z. Yang, Y. Xu, Y. Su, R. Li, M. Smidman, M. Wang, L. Jiao, and H. Yuan, High-temperature superconductivity with zero resistance and strange-metal behaviour in $\text{La}_3\text{Ni}_2\text{O}_{7-\delta}$, *Nat. Phys.* **20**, 1269 (2024).
- [4] J. Hou, P.-T. Yang, Z.-Y. Liu, J.-Y. Li, P.-F. Shan, L. Ma, G. Wang, N.-N. Wang, H.-Z. Guo, J.-P. Sun, Y. Uwatoko, M. Wang, G.-M. Zhang, B.-S. Wang, and J.-G. Cheng, Emergence of high-temperature superconducting phase in pressurized $\text{La}_3\text{Ni}_2\text{O}_7$ crystals, *Chin. Phys. Lett.* **40**, 117302 (2023).
- [5] G. Wang, N. N. Wang, X. L. Shen, J. Hou, L. Ma, L. F. Shi, Z. A. Ren, Y. D. Gu, H. M. Ma, P. T. Yang, Z. Y. Liu, H. Z. Guo, J. P. Sun, G. M. Zhang, S. Calder, J.-Q. Yan, B. S. Wang, Y. Uwatoko, and J.-G. Cheng, Pressure-induced superconductivity in polycrystalline $\text{La}_3\text{Ni}_2\text{O}_{7-\delta}$, *Phys. Rev. X* **14**, 011040 (2024).
- [6] Y. Zhou, J. Guo, S. Cai, H. Sun, P. Wang, J. Zhao, J. Han, X. Chen, Y. Chen, Q. Wu, Y. Ding, T. Xiang, H. Kwang Mao, and L. Sun, Evidence of filamentary superconductivity in pressurized $\text{La}_3\text{Ni}_2\text{O}_7$ single crystals, [arXiv:2311.12361](https://arxiv.org/abs/2311.12361).
- [7] M. Zhang, C. Pei, Q. Wang, Y. Zhao, C. Li, W. Cao, S. Zhu, J. Wu, and Y. Qi, Effects of pressure and doping on Ruddlesden-Popper phases $\text{La}_{n+1}\text{Ni}_n\text{O}_{3n+1}$, *J. Mater. Sci. Technol.* **185**, 147 (2024).
- [8] M. Wang, H.-H. Wen, T. Wu, D.-X. Yao, and T. Xiang, Normal and superconducting properties of $\text{La}_3\text{Ni}_2\text{O}_7$, *Chin. Phys. Lett.* **41**, 077402 (2024).
- [9] J. Li, P. Ma, H. Zhang, X. Huang, C. Huang, M. Huo, D. Hu, Z. Dong, C. He, J. Liao, X. Chen, T. Xie, H. Sun, and M. Wang, Pressure-driven dome-shaped superconductivity in bilayer nickelate $\text{La}_3\text{Ni}_2\text{O}_7$, [arXiv:2404.11369](https://arxiv.org/abs/2404.11369).
- [10] L. Wang, Y. Li, S.-Y. Xie, F. Liu, H. Sun, C. Huang, Y. Gao, T. Nakagawa, B. Fu, B. Dong, Z. Cao, R. Yu, S. I. Kawaguchi, H. Kadobayashi, M. Wang, C. Jin, H.-k. Mao, and H. Liu, Structure responsible for the superconducting state in $\text{La}_3\text{Ni}_2\text{O}_7$ at high-pressure and low-temperature conditions, *J. Am. Chem. Soc.* **146**, 10.1021/jacs.3c13094 (2024).
- [11] X. Chen, J. Choi, Z. Jiang, J. Mei, K. Jiang, J. Li, S. Agrestini, M. Garcia-Fernandez, X. Huang, H. Sun, D. Shen, M. Wang, J. Hu, Y. Lu, K.-J. Zhou, and D. Feng, Electronic and magnetic excitations in $\text{La}_3\text{Ni}_2\text{O}_7$, *Nat. Commun.* **15**, 9597 (2024).
- [12] K. Chen, X. Liu, J. Jiao, M. Zou, C. Jiang, X. Li, Y. Luo, Q. Wu, N. Zhang, Y. Guo, and L. Shu, Evidence of spin density waves in $\text{La}_3\text{Ni}_2\text{O}_{7-\delta}$, *Phys. Rev. Lett.* **132**, 256503 (2024).
- [13] R. Khasanov, T. J. Hicken, D. J. Gawryluk, L. P. Sorel, S. Bötzel, F. Lechermann, I. M. Eremin, H. Luetkens, and Z. Guguchia, Pressure-induced split of the density wave transitions in $\text{La}_3\text{Ni}_2\text{O}_{7-\delta}$, [arXiv:2402.10485](https://arxiv.org/abs/2402.10485).
- [14] Z. Dan, Y. Zhou, M. Huo, Y. Wang, L. Nie, M. Wang, T. Wu, and X. Chen, Spin-density-wave transition in double-layer nickelate $\text{La}_3\text{Ni}_2\text{O}_7$, [arXiv:2402.03952](https://arxiv.org/abs/2402.03952).

- [15] M. Kakoi, T. Oi, Y. Ohshita, M. Yashima, K. Kuroki, T. Kato, H. Takahashi, S. Ishiwata, Y. Adachi, N. Hatada, T. Uda, and H. Mukuda, Multiband metallic ground state in multilayered nickelates $\text{La}_3\text{Ni}_2\text{O}_7$ and $\text{La}_4\text{Ni}_3\text{O}_{10}$ probed by ^{139}La -NMR at ambient pressure, *J. Phys. Soc. Jpn.* **93**, 053702 (2023).
- [16] T. Xie, M. Huo, X. Ni, F. Shen, X. Huang, H. Sun, H. C. Walker, D. Adroja, D. Yu, B. Shen, L. He, K. Cao, and M. Wang, Neutron scattering studies on the high- T_c superconductor $\text{La}_3\text{Ni}_2\text{O}_{7-\delta}$ at ambient pressure, *Science Bulletin* **69**, 3221 (2024).
- [17] Z. Liu, M. Huo, J. Li, Q. Li, Y. Liu, Y. Dai, X. Zhou, J. Hao, Y. Lu, M. Wang, and H.-H. Wen, Electronic correlations and partial gap in the bilayer nickelate $\text{La}_3\text{Ni}_2\text{O}_7$, *Nat. Commun.* **15**, 7570 (2024).
- [18] Z. Liu, H. Sun, M. Huo, X. Ma, Y. Ji, E. Yi, L. Li, H. Liu, J. Yu, Z. Zhang, Z. Chen, F. Liang, H. Dong, H. Guo, D. Zhong, B. Shen, S. Li, and M. Wang, Evidence for charge and spin density waves in single crystals of $\text{La}_3\text{Ni}_2\text{O}_7$ and $\text{La}_3\text{Ni}_2\text{O}_6$, *Sci. China Phys. Mech. Astron.* **66**, 217411 (2022).
- [19] V. Christiansson, F. Petocchi, and P. Werner, Correlated electronic structure of $\text{La}_3\text{Ni}_2\text{O}_7$ under pressure, *Phys. Rev. Lett.* **131**, 206501 (2023).
- [20] X. Sui, X. Han, H. Jin, X. Chen, L. Qiao, X. Shao, and B. Huang, Electronic properties of the bilayer nickelates $R_3\text{Ni}_2\text{O}_7$ with oxygen vacancies ($R = \text{La}$ or Ce), *Phys. Rev. B* **109**, 205156 (2024).
- [21] Y. Cao and Y.-f. Yang, Flat bands promoted by Hund's rule coupling in the candidate double-layer high-temperature superconductor $\text{La}_3\text{Ni}_2\text{O}_7$ under high pressure, *Phys. Rev. B* **109**, L081105 (2024).
- [22] Z. Luo, X. Hu, M. Wang, W. Wú, and D.-X. Yao, Bilayer two-orbital model of $\text{La}_3\text{Ni}_2\text{O}_7$ under pressure, *Phys. Rev. Lett.* **131**, 126001 (2023).
- [23] Y. Zhang, L.-F. Lin, A. Moreo, and E. Dagotto, Electronic structure, dimer physics, orbital-selective behavior, and magnetic tendencies in the bilayer nickelate superconductor $\text{La}_3\text{Ni}_2\text{O}_7$ under pressure, *Phys. Rev. B* **108**, L180510 (2023).
- [24] F. Lechermann, J. Gondolf, S. Bötzel, and I. M. Eremin, Electronic correlations and superconducting instability in $\text{La}_3\text{Ni}_2\text{O}_7$ under high pressure, *Phys. Rev. B* **108**, L201121 (2023).
- [25] Y. Wang, K. Jiang, Z. Wang, F.-C. Zhang, and J. Hu, The electronic and magnetic structures of bilayer $\text{La}_3\text{Ni}_2\text{O}_7$ at ambient pressure, *Phys. Rev. B* **110**, 205122 (2024).
- [26] Z. Fan, J.-F. Zhang, B. Zhan, D. Lv, X.-Y. Jiang, B. Normand, and T. Xiang, Superconductivity in nickelate and cuprate superconductors with strong bilayer coupling, *Phys. Rev. B* **110**, 024514 (2024).
- [27] C. Lu, Z. Pan, F. Yang, and C. Wu, Interlayer-coupling-driven high-temperature superconductivity in $\text{La}_3\text{Ni}_2\text{O}_7$ under pressure, *Phys. Rev. Lett.* **132**, 146002 (2024).
- [28] Q.-G. Yang, D. Wang, and Q.-H. Wang, Possible s_{\pm} -wave superconductivity in $\text{La}_3\text{Ni}_2\text{O}_7$, *Phys. Rev. B* **108**, L140505 (2023).
- [29] Q. Qin and Y.-f. Yang, High- T_c superconductivity by mobilizing local spin singlets and possible route to higher T_c in pressurized $\text{La}_3\text{Ni}_2\text{O}_7$, *Phys. Rev. B* **108**, L140504 (2023).
- [30] Y.-f. Yang, G.-M. Zhang, and F.-C. Zhang, Interlayer valence bonds and two-component theory for high- T_c superconductivity of $\text{La}_3\text{Ni}_2\text{O}_7$ under pressure, *Phys. Rev. B* **108**, L201108 (2023).
- [31] Y.-B. Liu, J.-W. Mei, F. Ye, W.-Q. Chen, and F. Yang, s_{\pm} -wave pairing and the destructive role of apical-oxygen deficiencies in $\text{La}_3\text{Ni}_2\text{O}_7$ under pressure, *Phys. Rev. Lett.* **131**, 236002 (2023).
- [32] Y. Zhang, L.-F. Lin, A. Moreo, T. A. Maier, and E. Dagotto, Trends in electronic structures and s_{\pm} -wave pairing for the rare-earth series in bilayer nickelate superconductor $R_3\text{Ni}_2\text{O}_7$, *Phys. Rev. B* **108**, 165141 (2023).
- [33] Z. Liao, L. Chen, G. Duan, Y. Wang, C. Liu, R. Yu, and Q. Si, Electron correlations and superconductivity in $\text{La}_3\text{Ni}_2\text{O}_7$ under pressure tuning, *Phys. Rev. B* **108**, 214522 (2023).
- [34] Y. Gu, C. Le, Z. Yang, X. Wu, and J. Hu, Effective model and pairing tendency in bilayer Ni-based superconductor $\text{La}_3\text{Ni}_2\text{O}_7$, [arXiv:2306.07275](https://arxiv.org/abs/2306.07275).
- [35] H. Sakakibara, N. Kitamine, M. Ochi, and K. Kuroki, Possible high T_c superconductivity in $\text{La}_3\text{Ni}_2\text{O}_7$ under high pressure through manifestation of a nearly half-filled bilayer hubbard model, *Phys. Rev. Lett.* **132**, 106002 (2024).
- [36] X.-Z. Qu, D.-W. Qu, J. Chen, C. Wu, F. Yang, W. Li, and G. Su, Bilayer $t-J-J_{\perp}$ model and magnetically mediated pairing in the pressurized nickelate $\text{La}_3\text{Ni}_2\text{O}_7$, *Phys. Rev. Lett.* **132**, 036502 (2024).
- [37] Y.-H. Tian, Y. Chen, J.-M. Wang, R.-Q. He, and Z.-Y. Lu, Correlation effects and concomitant two-orbital s_{\pm} -wave superconductivity in $\text{La}_3\text{Ni}_2\text{O}_7$ under high pressure, *Phys. Rev. B* **109**, 165154 (2024).
- [38] Y.-Y. Zheng and W. Wú, Superconductivity in the bilayer two-orbital hubbard model, *Phys. Rev. B* **111**, 035108 (2025).
- [39] Z. Luo, B. Lv, M. Wang, W. Wú, and D.-X. Yao, High- T_c superconductivity in $\text{La}_3\text{Ni}_2\text{O}_7$ based on the bilayer two-orbital t - J model, *npj Quantum Mater.* **9**, 61 (2024).
- [40] S. Ryee, N. Witt, and T. O. Wehling, Quenched pair breaking by interlayer correlations as a key to superconductivity in $\text{La}_3\text{Ni}_2\text{O}_7$, *Phys. Rev. Lett.* **133**, 096002 (2024).
- [41] K.-Y. Jiang, Y.-H. Cao, Q.-G. Yang, H.-Y. Lu, and Q.-H. Wang, Theory of pressure dependence of superconductivity in bilayer nickelate $\text{La}_3\text{Ni}_2\text{O}_7$, [arXiv:2409.17861](https://arxiv.org/abs/2409.17861).
- [42] J. Huang, Z. D. Wang, and T. Zhou, Impurity and vortex states in the bilayer high-temperature superconductor $\text{La}_3\text{Ni}_2\text{O}_7$, *Phys. Rev. B* **108**, 174501 (2023).
- [43] K. Jiang, Z. Wang, and F.-C. Zhang, High-temperature superconductivity in $\text{La}_3\text{Ni}_2\text{O}_7$, *Chin. Phys. Lett.* **41**, 017402 (2024).
- [44] G. Heier, K. Park, and S. Y. Savrasov, Competing d_{xy} and s_{\pm} pairing symmetries in superconducting $\text{La}_3\text{Ni}_2\text{O}_7$: LDA + FLEX calculations, *Phys. Rev. B* **109**, 104508 (2024).
- [45] R. Jiang, J. Hou, Z. Fan, Z.-J. Lang, and W. Ku, Pressure driven fractionalization of ionic spins results in cuprate-like high- T_c superconductivity in $\text{La}_3\text{Ni}_2\text{O}_7$, *Phys. Rev. Lett.* **132**, 126503 (2024).
- [46] Y. Shen, M. Qin, and G.-M. Zhang, Effective bilayer model hamiltonian and density-matrix renormalization group study for the high- T_c superconductivity in $\text{La}_3\text{Ni}_2\text{O}_7$ under high pressure, *Chin. Phys. Lett.* **40**, 127401 (2023).
- [47] C. Xia, H. Liu, S. Zhou, and H. Chen, Sensitive dependence of pairing symmetry on $\text{Ni-}e_g$ crystal field splitting

- in the nickelate superconductor $\text{La}_3\text{Ni}_2\text{O}_7$, [Nat. Commun. **16**, 1054 \(2025\)](#).
- [48] N. E. Bickers and D. J. Scalapino, Conserving approximations for strongly fluctuating electron systems. I. Formalism and calculational approach, [Ann. Phys. **193**, 206 \(1989\)](#).
- [49] S.-L. Yu and J.-X. Li, Spin fluctuations and unconventional superconducting pairing in iron-based superconductors, [Chin. Phys. B **22**, 087411 \(2013\)](#).
- [50] H. Wang, S.-L. Yu, and J.-X. Li, Fermi arcs, pseudogap, and collective excitations in doped Sr_2IrO_4 : A generalized fluctuation exchange study, [Phys. Rev. B **91**, 165138 \(2015\)](#).
- [51] Z.-J. Yao, J.-X. Li, and Z. D. Wang, Spin Fluctuations, Interband Coupling and Unconventional Pairing in Iron-Based Superconductors, [New J. Phys. **11**, 025009 \(2009\)](#).